Journal of Materials Chemistry A

Accepted Manuscript

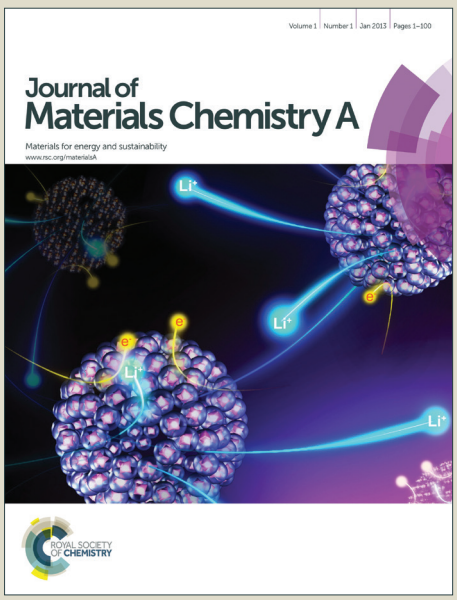

ROYAL SOCIETY OF CHEMISTRY

www.rsc.org/materialsA

Journal of Materials Chemistry A

Dynamic Article Links ►

Cite this: DOI: 10.1039/c0xx00000x

www.rsc.org/xxxxxx

ARTICLE TYPE

Advanced H_2-Storage System Fabricated Through Chemical Layer Deposition in a Well-Designed Porous Carbon Scaffold

Yanhui Guo,[a] Minghong Wang,[b] Guanglin Xia,[a] Xiaohua Ma,[a,c] Fang Fang*, [a] and Yonghui Deng*,[b]

Received (in XXX, XXX) Xth XXXXXXXXX 20XX, Accepted Xth XXXXXXXXX 20XX

DOI: 10.1039/b000000x

A new and effective *in-situ* impregnation/deposition technique of chemical layer deposition (CLD) on gas-solid interface is developed for fast and controllable film deposition and functional nanostructure design. Using CLD, a series of nanostructured $Al(BH_4)_3(NH_3)_6$@porous carbon composites are successfully produced, and a significant improvement of the hydrogen storage properties of $Al(BH_4)_3(NH_3)_6$ is achieved with tunable dehydrogenation temperature ranging from 114 to 175 °C, enhanced dehydrogenation kinetics with a low activation energy of 65.6 KJ/mol compared to 105.5 KJ/mol for the bulk counterpart, and a significant increased H_2 purity from 67.4 % to 93.5 %.

Introduction

Storing hydrogen in a dense form has been one of the critical obstacles toward the advantageous option of hydrogen based economy- a clean and sustainable energy future. To overcome this obstacle, a great variety of hydrogen storage materials (HSMs) have been developed.[1] To date, however, none of these candidates has met all the H_2 storage targets, and a practical solution is still in urgent demand.

To produce HSMs with promoted properties, various approaches including catalytic doping, ion substitution and size effect have been tried. Among them, size effect has been currently demonstrated to have a significant impact on HSM's hydrogen storage performances. Hence, HSMs with different nano-structure, such as nanowire, thin film, etc.,[2] are produced to utilize the size effect, and a large extension of hydrogen desorption kinetics and/or the thermodynamic properties has been achieved. Unfortunately, the dramatic hydrogen storage properties of nanostructured HSMs would rapidly degenerate upon de-/hydrogenation due to particle aggregation that blunts the size effect. To overcome this problem, HSMs are impregnated and confined in porous scaffolds to maintain the nanoscale particles during de-/hydrogenation. To data, the promotion of hydrogen storage properties has been achieved on several confined HSM systems, such as metal hydrides,[3] amine borane complexes,[4] etc..[5] However, current methods to produce the confined HSMs are rather limited. The two main choices for impregnation are melting infiltration and solvent mediated infiltration. They suffer intrinsic drawbacks of difficulty in gap filling of scaffolds with complex nanostructures, and the formation of large HSM particles on the external surfaces of the scaffold which results in uncertain amount of confined HSMs and complicated de-/hydrogenation processes. Moreover, the melting infiltration requires that both the HSM and scaffold remain stable at the melting point of HSMs, while the solvent mediated infiltration requires special solvents to dissolve HSMs which weakly coordinates to both HSM and scaffold.[5] These limitations make the infiltration methods less effective and even unsuitable for those HSM systems with low decomposition temperature and/or poor solution characteristics.[5b]

$Al(BH_4)_3(NH_3)_6$ (HAAB) is one of the most hydrogen abundant promising HSMs, however, its practical applications are hindered by unfavorable dehydrogenation kinetics and NH_3 impurity emission.[6] To alleviate these problems, size effect is expected to be beneficial. However, HAAB is exactly the sort of HSMs with low decomposition temperature and poor solution characteristics, thus it is impossible to produce confined HAAB via the traditional method. Recently, Yu et al. have successfully prepared confined HAAB in poly styrene-co-divinyl benzene (PSDB) using $Al(BH_4)_3$ and NH_3 gases. PSDB first absorbs $Al(BH_4)_3$ via the interaction of phenyl rings and Al^{3+} in $Al(BH_4)_3$ and then absorbs ammonia to yield the confined HAAB.[7] Since the gas diffusion in complex scaffolds is much easier and faster than liquid diffusion, the complex scaffolds with smaller pore can be used to load HSMs by gas impregnation to obtain smaller particles. However, precisely control of the HSM particle size is still difficult and the templating effect[7] from PSDB is apparent, resulting in a wide distribution of particle size and an ambiguous relationship between particle size and hydrogen storage performance. Thus, the development of novel deposition technique for facile synthesis of nanostructured HSMs is desired to exert the full potential of size effect, serve and strengthen the development of clean H_2 energy.

Herein, we demonstrate a novel method of chemical layer deposition (CLD) to deposit HAAB thin films with controllable thicknesses inside a complex scaffold to investigate the influence of size effect on its hydrogen storage properties. An inert hierarchically ordered macro-/meso-porous carbon (HOPC) was firstly prepared and used as the scaffold to produce confined HAAB (HAAB@HOPC). Using CLD, a series of fine

nanostructured HAAB@HOPC composites were synthesized, and their hydrogen storage properties were investigated. For the confined HAAB, a large extension of hydrogen storage properties- dehydrogenation peak temperature being tunable within 114 ~ 175 °C, remarkable enhancement of dehydrogenation kinetics, and NH_3 impurity suppression - have been achieved through the size effect. The results show that CLD is an effective impregnation method to produce nanostructured HSM with a homogeneous distribution, enabling simple regulation of hydrogen storage properties by particle size adjustment.

Experimental

Reagents and synthesis

The raw materials were obtained commercially, Pluronic® block copolymers poly (propylene oxide)-block-poly (ethylene oxide)-block-poly (propylene oxide) (F127, M_w = 12600, $EO_{106}PO_{70}EO_{106}$), $LiBH_4$ (95 %), Al powder (99 %) and $AlCl_3$ (99.999 %) were purchased from Sigma-Aldrich and used as received. NH_3 was purified by soda lime when using. Phenol (AR), formaldehyde solution (37 wt.%), tetraethyl orthosilicate (TEOS) (AR), ethanol and concentrated ammonia solution (28 wt.%), sodium hydroxide were purchased from Shanghai Chemical Corp. Resol, a soluble phenolic resin with low molecular weight (~ 500 g/mol) was prepared according to previous report.[8] In order to prevent contamination with air, all handling and manipulation for the chemicals, except for ammonia- related procedures, was performed in argon-filled glove box with a recirculation system to keep H_2O and O_2 levels below 1 ppm.

Preparation of carbon templates. Macro-mesoporous carbon materials were synthesized by using silica colloidal crystals as the templates, resol as carbon resource and F127 as the structure-directing agents. In a typical procedure, monodisperse silica spheres with diameters of 250±10nm (Supporting Information, Fig. S1) were obtained by using Stöber method [9] and washed with deionized water and ethanol for at least three times respectively. The purified silica spheres were dispersed in ethanol in a sealed flat bottom flask for 7 days to form colloidal crystals sediment. After the supernatant liquor was pumped out, the left solvent was evaporated for 12 h at 30 °C and the bulks were further heated at 100 °C for 12 h. An ethanol solution of resol and F127 (mass ratio of resol: F127: ethanol is 2:1:7) was dropped slowly and immersed the treated silica colloidal crystal for 24 h at 30 °C. After evaporation of ethanol, the composite products were put in an oven at 100 °C for 6 h to further polymerize resol. Calcination of the obtained silica/PF/F127 complexes in nitrogen at 600 °C for 3 h using a 3 °C/min hearting rate, nonionic surfactant F127 was decomposed. The resulting silica/carbon composites were then treated with hydrofluoric acid (4%) for 24 h to etch the silica spheres, followed by washing with water and ethanol for three times respectively and dried at 50 °C in a vacuum oven for 24 h. Nitrogen adsorption-desorption isotherms (Fig. S2) of the samples shows that the materials possess high BET surface area of 980 m^2/g, large pore volume of 1.629 cm^3/g and mesopore size of 12.7 nm.

Preparation of HAAB confined into templates via CLD. Carbon scaffolds (250nm) were first heated at 400 °C in vacuum for around 3 h to remove moisture and gases that adsorbed in the porous structure. Before loading, the entire system (Fig. S3) was dried by thorough evacuation and then refilled with dry argon for three times. The source of $Al(BH_4)_3$ gas ($AlCl_3$:$LiBH_4$:Al=2.2:1:2, 30 °C) and the carbon templates are placed separately in the different reaction tube. To produce confined $Al(BH_4)_3(NH_3)_6$, NH_3 was first incorporated into carbon templates by physical adsorption at room temperature for 15 min, followed with 10 min evaporation via dynamic vacuum to remove free gases in scaffolds. Afterwards, the reaction tube was refilled with $Al(BH_4)_3$-N_2 mixture produced by the $Al(BH_4)_3$ source reactor and stand for 15 min, within this period the given amount of $Al(BH_4)_3$ in the tube will react with the adsorbed NH_3 to produce $Al(BH_4)_3(NH_3)_x$ ($0<x<6$) inside the pores of carbon templates. This process was repeated several times until the capacity of $Al(BH_4)_3(NH_3)_x$ reached the targeted loading of the composites. Finally, the product was kept in ammonia overnight and then vacuum for around 5 h to produce confined $Al(BH_4)_3(NH_3)_6$ composites. The increasing weight of the product was monitored by weighting reactor B shown in Fig. S3 during the experiment for process control. Composites with nominal $Al(BH_4)_3(NH_3)_6$ loadings of approximately 20, 30, 40, and 50 wt.% were prepared and the samples were denoted as C-X, in which X stands for the weight percentage of $Al(BH_4)_3(NH_3)_6$ in the composite. Physical mixtures were prepared by mixing $Al(BH_4)_3(NH_3)_6$ with dried carbon templates with a weight ratio of 30 wt.% by handy milling. $Al(BH_4)_3(NH_3)_5$@HOPC was synthesized via further deposition of a certain amount of $Al(BH_4)_3$ into C-30 sample via CLD to reduce the coordination number of HAAB from 6 to 5.

Deposition of HAAB on a quartz crystal (QC) and silicon slice. The source of $Al(BH_4)_3$ gas ($AlCl_3$:$LiBH_4$:Al=2.2:1:2, 30 °C) and the quartz crystal together with silicon slice are placed separately in the different reaction tube. Quartz crystal was connected with a quartz-crystal resonator to monitor the tiny mass change of an added film. Before loading, the entire system (Fig. S3) was dried by thorough evacuation for 30min. Then, NH_3 was first incorporated into the reaction chamber at around 15 °C for 5 min to activate the surface. After 10 min evaporation via dynamic vacuum, Plenty of $Al(BH_4)_3$ was introduced into the reaction tube for a certain time until no weight increase was observed by QCM method. Subsequently, the excess $Al(BH_4)_3$ was pumped out and then NH_3 was injected into reaction tube to produce $Al(BH_4)_3(NH_3)_6$. This treatment was repeated for several times until the total weight of HAAB reaches the set value. It is worth noting that $Al(BH_4)_3$ is extremely reactive and very easy to self-ignite in contact with air and moisture.

Instrumentation and analyses

The QCM method described by Sauerbrey is generally used to measure tiny mass change of an added film by using a quartz-crystal resonator.[10] The change in resonance frequency is proportional to the mass of an added film:

$$\Delta f = \frac{-2f_0^2}{\sqrt{\mu_q \rho_q}} \frac{\Delta m}{A} \qquad (1)$$

where Δf is the measured frequency change (Hz), f_0 is the fundamental frequency of quartz crystal (Hz), A is the electrochemically and piezoelectrically active surface area of the quartz crystal (cm^2), ρ_q is the density of quartz (2.648 g/cm^3),

and μ_q is the shear modulus of quartz ($2.947*10^{11}$ g/cm·s^2). For the quartz crystal used here (f_0 = 6 MHz, A = 0.4*0.4*π*2 cm^2), the relationship between the frequency shift (Δf, Hz) and mass change (Δm, μg) is simply expressed as follows:

$$\Delta f = -81.07 * \Delta m \quad (2)$$

Nitrogen sorption isotherms were measured at 77 K with a Micromeritics Tristar 3020 analyzer (USA). Before measurements, the samples were degassed in a vacuum at 180 °C for at least 6 h. The Brunauer–Emmett–Teller (BET) method was utilized to calculate the specific surface areas. By using the Barrett-Joyner-Halenda (BJH) model, the pore volumes and pore size distributions were derived from the adsorption branches of isotherms, and the total pore volumes (Vt) were estimated from the adsorbed amount at a relative pressure P/P_0 of 0.992. Transmission electron microscopy (TEM) experiments were conducted on a JEOL 2011 microscope (Japan) operated at 200 kV. Field-emission scanning electron microscopy (FESEM) images were collected on the Hitachi Model S-4800 field emission scanning electron microscope. The dried samples were directly used for the observation without any treatment.

Simultaneous thermo-gravimetric analysis and mass spectrometry (TGA-MS, TA Q500-Hiden QIC 20) were conducted from room temperature using a heating rate of 5 ^oC min^{-1} under 1 atm dynamic nitrogen with a purge rate of 150 ml min^{-1}. Typical sample quantities were 5-10 mg. Volumetric release for quantitative measurements of the hydrogen desorption from the samples was carried out on a home-made Sieverts' type apparatus under 1 atm Ar atmosphere. The desorption properties of some samples were also evaluated using Sieverts' volumetric method with a heating rate of 5 ^oC min^{-1} and at varied isothermal temperatures under argon atmosphere. The phase composition of the powders was analyzed by X-ray diffraction (D8 Advance, Bruker AXS) with Cu Kα radiation. Amorphous tape was used to prevent any possible reactions between sample and air during the XRD measurements. FTIR (Magna-IR 550 II, Nicolet) analysis was conducted to determine the chemical bonding. During the IR measurements (KBr pellets), samples were loaded into a closed tube with KBr for measurements in an argon-filled glovebox. The contents of H_2 and NH_3 in the emission gas were determined based on the combination of gravimetric and volumetric results. Firstly, the mass percent (W_p) and mole per gram (M_p) of the gas released from the sample were calculated from the weights of the samples and volumetric results. For the product that mainly released H_2 and NH_3, the mole proportion of H_2 (C_{H2}) and NH_3 (C_{NH3}) can be calculated from equation (1) and (2).

$C_{H2} + C_{NH3} = 1$ (1)

$(C_{H2}*2.02 + C_{NH3}*17.03)*M_p = W_p$ (2)

Results and discussion

First of all, the inert HOPCs were synthesized via a dual soft/hard templating approach.[8] The synthesized HOPC materials have highly ordered 3-dimensional arrays of macropores (~ 250 nm) (Fig. 1), and all the macropores are well-connected by the large windows of ~ 70 nm in diameter (marked by arrows in Fig. 1). The magnified FESEM image clearly indicates that the macropores are surrounded by numerous uniform mesopores (about 12 nm). The hierarchically porous structure of the HOPCs is beneficial to the host-guest chemistry like storage and release of guest molecules, because the macropores interconnected by large windows can provide a fast mass transport, while the numerous mesopores in the macropore walls serve as branched channels to increase the diffusion rate for guest molecules. More importantly, the comparison of the decomposition properties of bulk HAAB and its physical mixture with the HOPCs (Fig. S4) shows that almost the same hydrogen evolution along with significant ammonia impurity emission proceeded in the temperature range of 120-220 ^oC (peaked at ~ 175 ^oC), indicating that the presence of HOPCs has little influence on the dehydrogenation behavior of HAAB. Therefore, in this case, HOPCs are chosen as an inert scaffold to investigate the size effect without the templating effects.

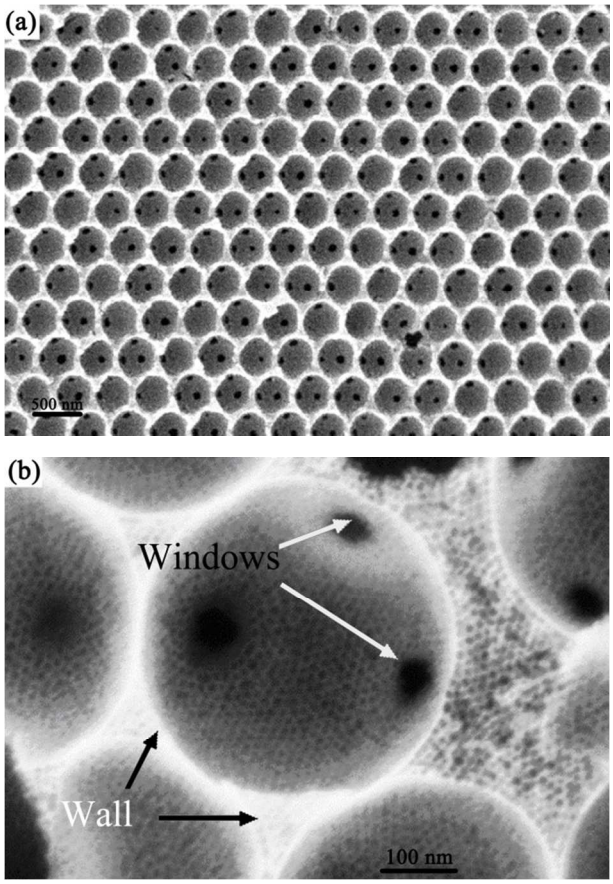

Fig.1 (a) SEM and (b) FESEM images for HOPC, large windows (about 70 nm) and sourounded by numerous mesopores (12.7 nm)

Using HOPC as a scaffold, chemical layer deposition (CLD) is proposed to produce HAAB@HOPC composites. The deposition of HAAB films inside HOPC involves two precursors, NH_3 and $Al(BH_4)_3$. They can spontaneously react on contact, producing a series of ammine aluminium borohydrides (AAB), formulated as $Al(BH_4)_3(NH_3)_{6-y}$ ($0 \le y < 6$).[11] In the CLD process, they are introduced into process chamber one-at-a-time alternately at 5-10 ^oC for a certain cycles (Fig. S3). Weight increments of the samples after each cycle shown in Fig. S5 clearly suggest the proceeding of the film deposition during the CLD process. The resulting HAAB@HOPC composites are denoted as C-X with X

standing for the weight percentage of HAAB in the composite.

High-resolution scanning electron microscope (HESEM) and transmission electron microscopy (TEM) observations (Fig. 2 and S6) further confirm the successful deposition of materials into the carbon scaffold. It is shown that after 6 cycles of deposition (~ 30 wt.%), the pores inside HOPC become small and few, and HAABs are exclusively deposited on the walls of HOPCs. More evident change is observed on the sample after 12 impregnation cycles (~ 40 wt.%), the mesopores are stuffed and the macropore windows become even smaller. It is worthy to be noted that no obvious aggregation of materials is observed on the surface of the scaffolds (Fig. S6). The composition of the loaded materials is identified to be HAAB by X-ray diffraction (Figure S7) as well as FT-IR spectra (Figure S8), confirming the successful deposition of HAAB into the complex scaffold via CLD method.

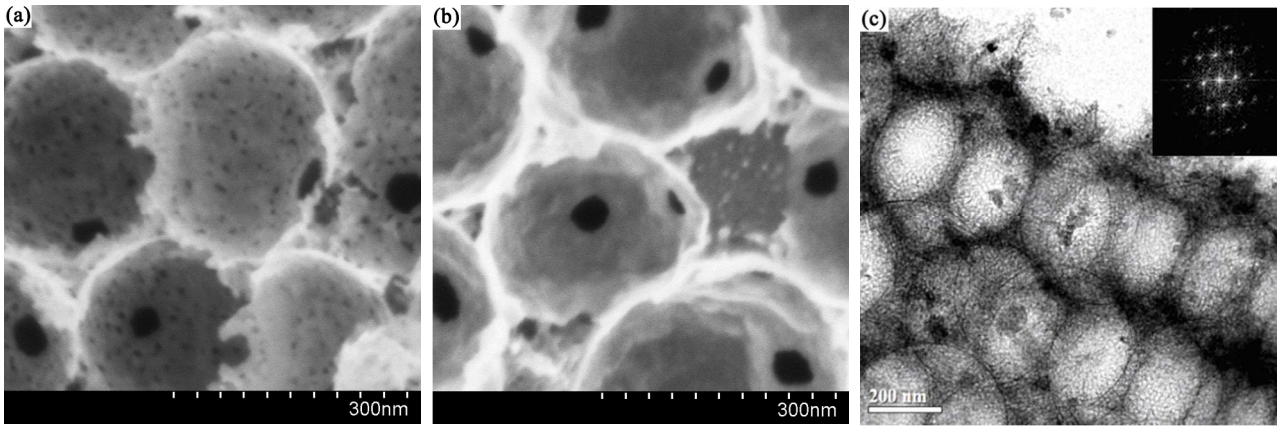

Fig. 2 (a) FESEM of the HAAB@HOPC composite after 6 cycles, (b) FESEM of the composite after 12 cycles, (c) TEM images of the composites after 6 cycles, taking along the [211] directions of the ordered arrays of macropores. The inset in part c is the corresponding Fourier transform (FFT) diffractograms.

To understand the film growth mechanism, the deposition process of HAAB on a quatz crystal plate (QC, diam., 8 mm) is *in-situ* investigated by quartz crystal microbalance (QCM) method (Fig. 3). The change of film weight is monitored during deposition process according to the variation of resonance frequency in resonant circuit. In cycle 0, the QC is first activated in ammonia, and 0.16 μg of NH_3 is adsorbed on its surface resulting in 13 Hz reduction of the QC frequency. Then, $Al(BH_4)_3$ is introduced onto the activated surface, and 0.33μg of $Al(BH_4)_3$ is absorbed by active QC substrate, corresponding to 27 Hz reduction of the QC frequency. The molecular formula of deposited AAB is calculated to be $Al(BH_4)_3(NH_3)_{2.01}$. Subsequent introduction of NH_3 into the chamber during cycle 1 transferred $Al(BH_4)_3(NH_3)_{2.01}$ to $Al(BH_4)_3(NH_3)_6$. During the following cycles, $Al(BH_4)_3$ and NH_3 are introduced onto the QC substrate alternately, and the absorption amount of both NH_3 and $Al(BH_4)_3$ almost triples after each cycle, suggesting that precursors react with not only the film surface but the whole layer, namely, mass transfer within the layer occurs. After 3 cycles, a HAAB film with a thickness of about 100 nm (inserted SEM image in Figure 3a) is deposited. According to the deposition weight, it can be calculated that the composition of the film alternates between $Al(BH_4)_3(NH_3)_{2\pm0.1}$ and $Al(BH_4)_3(NH_3)_6$ during the CLD process. Therefore, the proceeding of the film growth on QC in each cycle probably bases on reactions as follow:

(A) $Al(BH_4)_3(NH_3)_{2\pm0.1}$* $+NH_3 \rightarrow Al(BH_4)_3(NH_3)_6$*

(B) $Al(BH_4)_3(NH_3)_6$*$+ Al(BH_4)_3 \rightarrow Al(BH_4)_3(NH_3)_{2\pm0.1}$*

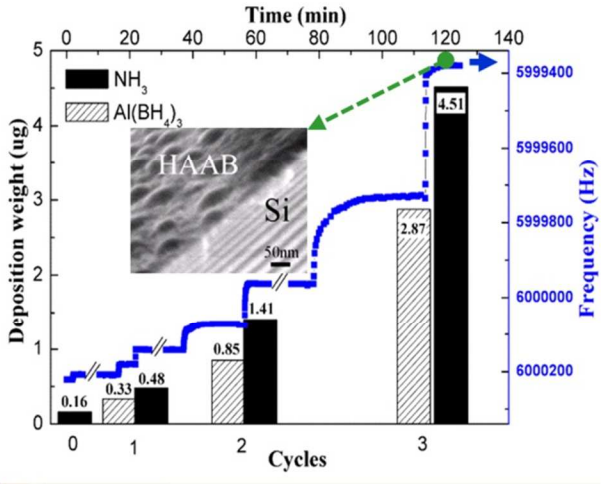

Fig.3 The growth manner of Chemical Layer Depostion process. (a) Deposition amount for each cycle during CLD process, inserted is FESEM image of the as-deposited HAAB/Silicon after 3 cycles.

Here the asterisks denote the film species.

Thus, for a growing HAAB film, upon contact with $Al(BH_4)_3$, the coordination number of the products is reduced. Oppositely, exposure to NH_3 atmosphere results in a higher coordination number of the whole film. The surface reaction as well as mass transfer within the layer occurs during preparation and the supposed procedure for deposition of HAAB is schematically illustrated in Fig. 4. More importantly, less deposition amount within its maximal value for each cycle is tunable by varying exposure time and/or precursor supply. A series of HAAB films with different thickness have been successfully prepared (Figure S9) by varying exposure time or increasing cycles, demonstrating the controllability of CLD method.

After the preparation of HAAB films with different thickness inside HOPCs, the dehydrogenation of HAAB@HOPC is investigated in detail using Fourier transform infrared (FTIR) spectrum, simultaneous thermo-gravimetric analysis-mass

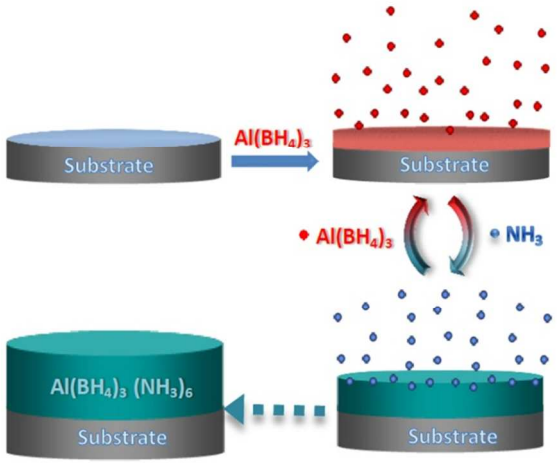

Fig. 4 Shematic diagram for deposition of $Al(BH_4)_3(NH_3)_6$ on substrate.

spectroscopy (TGA-MS) and the temperature-programmed-desorption (TPD) technique to further study the influence of size effect on hydrogen storage properties. For comparison, the measurement results of bulk HAAB are also presented. Typical FTIR results (Fig. S10) reveal that after heating to 160 °C, B-H and N-H bonds disappeared for the nanoconfined HAAB, indicating the participation of BH_4 groups and NH_3 groups towards H_2 release. This dehydrogenation phenomena is similar to the N-$H^{\delta+}\cdots H^{\delta-}$-B combination of bulk HAAB,[6] suggesting that the reduction of particle size has little influence on its dehydrogenation mechanism. Regarding to the dehydrogenation process, three remarkable improvements are observed with decreasing the weight percentage of HAAB in C-X composites, i.e., with decreasing the thickness of HAAB films: i) dehydrogenation results (Fig. 5a) shows that the peak temperatures for H_2 evolution are reduced with decreasing X. The peak temperature of C-50 is 153 °C, 22 °C lower than 175 °C of bulk HAAB. With the X decreases from 50 to 20, the peak temperatures fall from 153 °C to 114 °C; ii) MS results (Fig. 5a) demonstrate that the ammonia impurity emission from HAAB@HOPCs is significantly suppressed as compared to bulk HAAB. Quantitative analysis of the purities is provided by a combination of TGA and TPD results (Fig. S11). The analysis results (Fig. S12) show that the content of ammonia impurity decreases gradually from 32.6 wt.% for bulk HAAB, to 29.9 wt.% for C-50, 25.1 wt.% for C-40, 15.2 wt.% for C-30 and only 6.5 wt.% for C-20, respectively. Consequently, with decreasing the weight percentage of HAAB, more hydrogen is released as more ammonia participates in the dehydrogenation reaction instead of evolution; iii) the dehydrogenation kinetics is significantly improved. To quantitatively assess the enhancement of kinetics, isothermal TPD measurements at 80-110 °C are conducted, and the results for C-30 are shown in Fig. 5b as a typical sample. For bulk $Al(BH_4)_3(NH_3)_6$, no hydrogen liberation is observed at 90 °C, while for C-30, the weight loss reaches ~ 9.5 wt.% within 300 min at the same temperature. Activation energy calculated based on isothermal dehydrogenation is 39.9 KJ/mol for C-30, implying a considerable reduction of 65.6 KJ/mol as compared to 105.5 KJ/mol for the bulk HAAB. Although the kinetics is dramatically improved, the weight percentage of HAAB has no significant thermal effect on the dehydrogenation. Differential scanning calorimeter (DSC) results (Fig. S13 and Table S1) reveals that the dehydrogenation enthalpy of 6.78 KJ/mol H_2 for C-50 is similar with that of -6.75 KJ/mol H_2 for bulk HAAB and slightly reduced to -6.79 KJ/mol H_2, -6.79 KJ/mol H_2 and -7.23 KJ/mol H_2 for C-40, C-30 and C-20, respectively. It indicates that the dehydrogenation of samples with lower HAAB content is a little more exothermic. It may result from the full involvement of ammonia in an exothermic combination of N-H and B-H to produce H_2 rather than its endothermic emission.

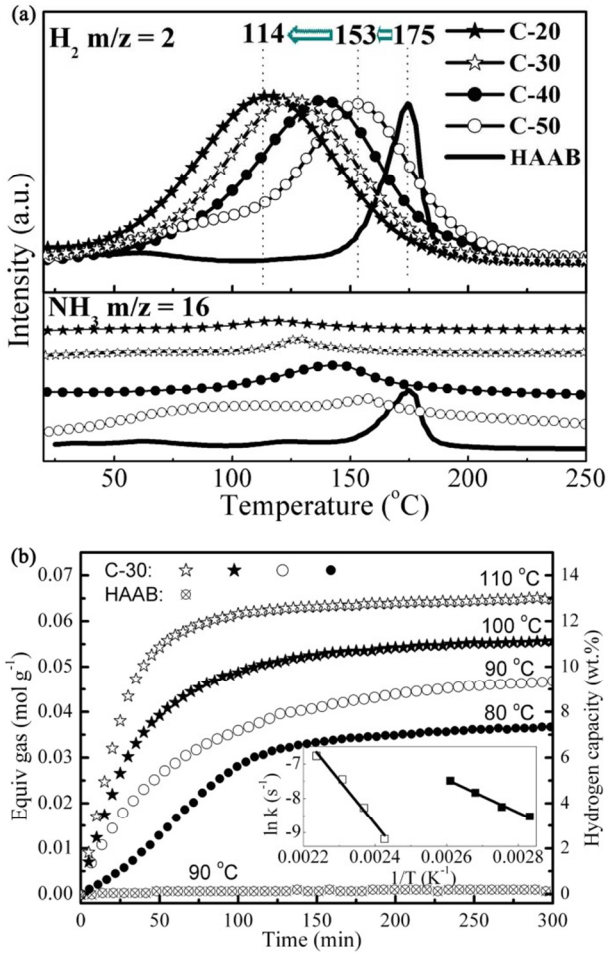

Fig. 5 (a) MS spectra of HAAB@HOPC (C-20, C-30, C-40, C-50) and bulk HAAB upon heating to 250 °C with a heating rate of 5 °C/min in N_2. (b) Isothermal TPD curves for the decomposition of C-30 and bulk $Al(BH_4)_3(NH_3)_6$, the inset was the Arrhenius treatment of bulk $Al(BH_4)_3(NH_3)_6$ (■) and C-30 (□).

Although significant improvement can be achieved for the dehydrogenation properties, complete suppression of ammonia seems impossible due to the high molar ratio (6:1) of NH_3 to $Al(BH_4)_3$ in HAAB@HOPC. Therefore, further deposition of a certain amount of $Al(BH_4)_3$ into C-30 sample using CLD was carried out to reduce the coordination number of HAAB from 6 to 5, yielding a composite of $Al(BH_4)_3(NH_3)_5$@HOPC. The dehydrogenation of $Al(BH_4)_3(NH_3)_5$@HOPC compared with that of C-30 and bulk $Al(BH_4)_3(NH_3)_5$ are shown in Fig. 6 and Fig. S14. Firstly, the reduction of coordination number from 6 to 5 in $Al(BH_4)_3(NH_3)_5$@HOPC not only lowers the dehydrogenation

peak temperature from 125 °C for C-30 to 109 °C but also leads to fairly pure hydrogen evolution. These improvements suggest the effectiveness of coordination number adjustment in promoting the dehydrogenation performance of AAB. Secondly, the dehydrogenation of $Al(BH_4)_3(NH_3)_5$@HOPC is also better than that of bulk $Al(BH_4)_3(NH_3)_5$ which releases hydrogen peaked at 159 °C with ammonia impurity emission, indicating the benefit of size effect.[11b] These results above further demonstrate the potential of CLD technique in deposition AAB film with tunable component besides tunable thickness. These advantages may make the CLD method attractive for confined HSM system exploration in the future.

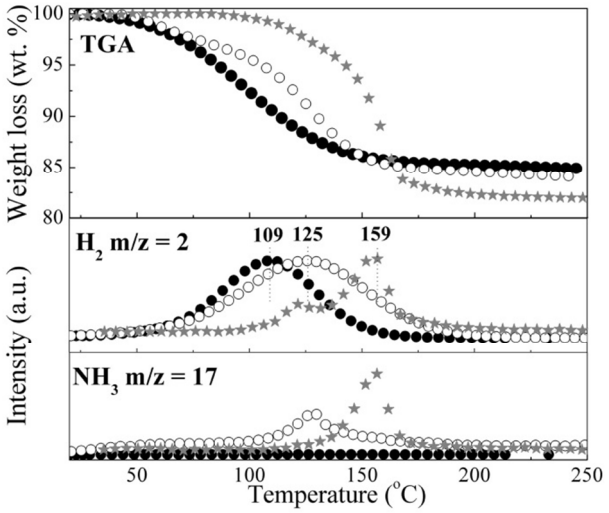

Fig. 6 TGA-MS spectra of $Al(BH_4)_3(NH_3)_5$@HOPC (●), bulk $Al(BH_4)_3(NH_3)_5$ (★) and C-30 (○).

Conclusions

In summary, we describe a novel deposition approach of chemical layer deposition (CLD) that enables effective fabrication of confined system for hydrogen storage. CLD is a facile technique for depositing films onto substrates based on two sequential and interdependent film growth processes. In each process, precursors react with the whole layer, thickening the film. Using CLD, ammine aluminum borohydride was successfully deposited in HOPC at a relatively fast speed, via alternant exposure to NH_3 and $Al(BH_4)_3$. The thickness of $Al(BH_4)_3(NH_3)_6$ layers has been well controlled through the reaction cycle number. Two notable improvements on the hydrogen desorption kinetics and ammonia impurity suppression exhibit for confined $Al(BH_4)_3(NH_3)_6$, realizing 7.3 wt.% relatively pure hydrogen at 80 °C within 300 min. Furthermore, the required two half reactions of CLD could also be achieved on several B-N-H systems, such as ammonia borane (two precursors of borane and ammonia) and its derivatives, hydrazine borane (two precursors of borane and hydrazine), and ammine metal borohydride (AMB) similar to $Al(BH_4)_3(NH_3)_6$, etc. Other HSM systems including borohydrides, alanates, amide, metal hydrides may also have the possibility after careful design the synthetic route using precursor, e.g. organic precursor. Meanwhile, besides single layer, the growth of different multilayer structures is also straight forward via CLD, enabling an easy design of hydrogen storage composites as well as other functional structures.

Acknowledgements

This work was partially supported by the National Natural S This work was financially supported by the State Key 973 Program of PRC (2013CB934104, 2012CB224805 and 2010CB631302), National Natural Science Foundation of China (U1201241, 51372041 and 51201035), the innovation program of Shanghai Municipal Education Commission (13ZZ004), Shanghai Rising Star Project of STCSM (12QH1400300), the Program for New Century Excellent Talents in Universities (NCET-08-0135, NCET-12-0123), the specialized research fund for the doctoral program of higher education of China (20120071110007, 20110071120008), and the ''Shu Guang'' Project (13SG02) supported by Shanghai Municipal Education Commission and Shanghai Education Development Foundation.

Notes and references

[a] Department of Materials Science, Fudan University, Shanghai, China, 200433.
[b] Department of Chemistry, State key Laboratory of Molecular Engineering of Polymers, Fudan University, Shanghai, 200433 China
c Center of Special Materials and Technology, Fudan University, Shanghai, 200433 China

† Electronic Supplementary Information (ESI) available: Experimental, Figures S1 to S14 and Table S1. See DOI: 10.1039/b000000x/

[1] L. Schlapbach, A. Zuttel, *Nature* 2001, **414**, 353-358; Z. T. Xiong, C. K. Yong, G. T. Wu, P. Chen, W. Shaw, A. Karkamkar, T. Autrey, M. O. Jones, S. R. Johnson, P. P. Edwards, W. I. F. David, *Nat. Mater.* 2008, **7**, 138-141; K. J. Jeon, H. R. Moon, A. M. Ruminski, B. Jiang, C. Kisielowski, R. Bardhan, J. J. Urban, *Nat. Mater.* 2011, **10**, 286-290; P. Chen, Z. T. Xiong, J. Z. Luo, J. Y. Lin, K. L. Tan, *Nature* 2002, **420**, 302-304; A. D. Sutton, A. K. Burrell, D. A. Dixon, E. B. Garner, J. C. Gordon, T. Nakagawa, K. C. Ott, P. Robinson, M. Vasiliu, *Science* 2011, **331**, 1426-1429; W. Grochala, P. P. Edwards, *Chem. Rev.* 2004, **104**, 1283-1315; S. I. Orimo, Y. Nakamori, J. R. Eliseo, A. Zuttel, C. M. Jensen, *Chem. Rev.* 2007, **107**, 4111-4132; A. Staubitz, A. P. M. Robertson, I. Manners, *Chem. Rev.* 2010, *110*, 4079-4124; J. Graetz, *Chemical Society Reviews* 2009, **38**, 73-82; J. Yang, A. Sudik, C. Wolverton, D. J. Siegel, *Chemical Society Reviews* 2010, **39**, 656-675.
[2] W. Li, C. Li, H. Ma, J. Chen, *J. Am. Chem. Soc.* 2007, **129**, 6710-6711; Y. Pang, Y. Liu, M. Gao, L. Ouyang, J. Liu, H. Wang, M. Zhu, H. Pan, *Nature communications* 2014, *10.1038/ncomms4519*; W. P. Kalisvaart, A. Kubis, M. Danaie, B. S. Amirkhiz, D. Mitlin, *Acta Mater.* 2011, **59**, 2083-2095.
[3] M. Fichtner, Z. Zhao-Karger, J. J. Hu, A. Roth, P. Weidler, *Nanotechnology* 2009, **20**, 5; N. S. Norberg, T. S. Arthur, S. J. Fredrick, A. L. Prieto, *J. Am. Chem. Soc.* 2011, **133**, 10679-10681; S. Cahen, J. B. Eymery, R. Janot, J. M. Tarascon, *J. Power Sources* 2009, **189**, 902-908; N. Brun, R. Janot, C. Sanchez, H. Deleuze, C. Gervais, M. Morcrette, R. Backov, *Energy Environ. Sci.* 2010, **3**, 824 - 830; S. Y. Zheng, F. Fang, G. Y. Zhou, G. R. Chen, L. Z. Ouyang, M. Zhu, D. L. Sun, *Chem. Mat.* 2008, **20**, 3954-3958; M. F. Ingleson, J. P. Barrio, J. Bacsa, A. Steiner, G. R. Darling, J. T. A. Jones, Y. Z. Khimyak, M. J. Rosseinsky, *Angew. Chem.-Int. Edit.* 2009, **48**, 2012-2016; X. F. Wan, L. L. Shaw, *Acta Mater.* 2011, **59**, 4606-4615; T. K. Nielsen, U. Bosenberg, R. Gosalawit, M. Dornheim, Y. Cerenius, F. Besenbacher, T. R. Jensen, *ACS Nano* 2010, **4**, 3903-3908.
[4] J. Z. Zhao, J. F. Shi, X. W. Zhang, F. Y. Cheng, J. Liang, Z. L. Tao, J. Chen, *Adv. Mater.* 2010, **22**, 394-397.
[5] H. Reardon, J. M. Hanlon, R. W. Hughes, A. Godula-Jopek, T. K. Mandal, D. H. Gregory, *Energy Environ. Sci.* 2012, **5**, 5951-5979; T. K. Nielsen, F. Besenbacher, T. R. Jensen, *Nanoscale* 2011, **3**, 2086-2098.
[6] Y. H. Guo, X. B. Yu, W. W. Sun, D. L. Sun, W. N. Yang, *Angew. Chem.-Int. Edit.* 2011, **50**, 1087-1091.

[7] Z. Tang, Y. Tan, X. Chen, L. Ouyang, M. Zhu, D. Sun, X. Yu, *Angewandte Chemie* 2013, **125**, 12891-12895.
[8] Y. Deng, C. Liu, T. Yu, F. Liu, F. Zhang, Y. Wan, L. Zhang, C. Wang, B. Tu, P. A. Webley, H. Wang, D. Zhao, *Chem. Mat.* 2007, **19**, 3271-3277.
[9] W. Stöber, A. Fink, E. Bohn, *J. Colloid Interface Sci.* 1968, **26**, 62-69.
[10] G. Sauerbrey, *Z. Physik* 1959, **155**, 206-222.
[11] J. C. Fauroux, S. J. Teichner, *Bull. Soc. Chim. Fr.* 1967, 4052-4055; Y. Guo, Y. Jiang, G. Xia, X. Yu, *Chem. Commun.* 2012, **48**, 4408-4410.

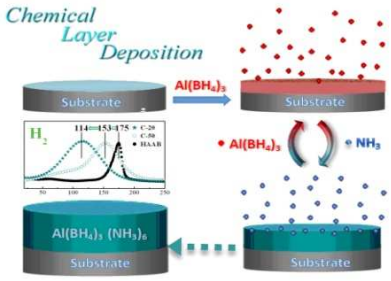

An effective chemical layer deposition (CLD) method is developed for fast and controllable film deposition of $Al(BH_4)_3(NH_3)_6$ for hydrogen storage.